Petroleum Science 22 (2025) 1214–1224

Contents lists available at ScienceDirect

Petroleum Science

journal homepage: www.keaipublishing.com/en/journals/petroleum-science

Original Paper

Experimental study of EOR mechanisms of non-chemical CO_2 microbubbles and their impact on pore structures

Hao-Wei Jia [a], Hai-Yang Yu [a, *], Rui Ma [a], Peng Song [b], Zhou Yuan [c], Jing-Pu Zhang [a], Tao Huang [a], Jun Lu [d], Yang Wang [a, **]

[a] State Key Laboratory of Petroleum Resources and Engineering, China University of Petroleum (Beijing), Beijing, 102249, China
[b] Research Institute of Exploration and Development, PetroChina Changqing Oilfield Company, Xi'an, 710018, Shaanxi, China
[c] SINOPEC Research Institute of Petroleum Engineering Co., Ltd, Beijing, 102206, China
[d] McDougall School of Petroleum Engineering, The University of Tulsa, Tulsa, OK, 74104, USA

ARTICLE INFO

Article history:
Received 16 April 2024
Received in revised form
3 January 2025
Accepted 3 January 2025
Available online 3 January 2025

Edited by Yan-Hua Sun

Keywords:
Non-chemical CO_2 microbubble
Low-permeability reservoir
Enhanced oil recovery
Nuclear magnetic resonance

ABSTRACT

Non-chemical CO_2 microbubbles as a mobility control technology in enhanced oil recovery (EOR) and carbon sequestration are becoming attractive. In this study, the EOR mechanisms of non-chemical CO_2 microbubble (MB) in low permeability reservoirs are experimentally investigated by the nuclear magnetic resonance (NMR) technology. This study reveals, for the first time, the EOR mechanisms of MB in a heterogeneous reservoir and its effect on pore structure. First, mobility reduction factors of MB with various gas–liquid ratios were determined, with MB at a gas–liquid ratio of 1 exhibiting the best performance under experimental conditions. Second, the coreflood experiments with NMR scanning were performed to reveal the EOR mechanisms of MB. It was observed that MB achieved an incremental oil recovery of 13.49% and 22.80% in the core sample with a permeability of 9.51×10^{-3} and 2.23×10^{-3} μm^2, respectively. Benefiting from MB's conformance control, the total oil recovery was increased from 38.34% to 54.57% of original oil in place by MB in parallel core flood experiments. Third, the NMR tests demonstrated that MB significantly reduced residual oil in core samples, especially in small pore areas, which highlights the improvement of sweep efficiency by MB. Lastly, the effect of MB on pore structure was studied. The NMR tests indicated a significant increase in pore space after 1 pore volume of MB flooding. Minerals in the core sample were dissolved, leading to an increase in permeability and porosity of the core sample by 17.01% and 0.31%, respectively. Overall, the results of this study provide valuable insights into the EOR mechanisms of MB at the pore scale and offer implications for EOR and carbon sequestration in low-permeability reservoirs.

1. Introduction

With the increasing fossil fuel consumption all over the world, CO_2 has been excessively emitted into the environment, which has led to global warming and other environmental problems (Jiménez-de-la-Cuesta and Mauritsen, 2019). Thus, carbon capture, utilization, and storage (CCUS) technologies are considered to be a solution to meet the world's carbon-neutral goals (Hasan et al., 2015; Hill et al., 2020). CO_2 enhanced oil recovery (CO_2-EOR) can storge CO_2 with a lot of revenue, which can further benefit the whole industry chain of CCUS projects (Ren et al., 2022; Sun and Chen, 2022; Liu et al., 2023). However, in low-permeability reservoirs, gas channeling, reservoir heterogeneity, and gravity segregation often lead to unfavorable oil recovery and significantly reduce the carbon sequestration ratio, which could damage the operation of the EOR project (Fang et al., 2019; Zhang et al., 2019; Yu et al., 2021a; Kang et al., 2022; Liu and Rui, 2022; Qi et al., 2022a, 2022b). To improve the performance of CO_2-EOR, technologies with conformance control ability are introduced, such as foam flooding, carbonate water flooding (Yu et al., 2019; Li S. et al., 2020; Tang et al., 2022), and water altering gas (Talebian et al., 2014; Ajayi et al., 2019). Foam flooding can effectively hinder gas breakthrough time and improve sweep efficiency, which has been

* Corresponding author.
** Corresponding author.
E-mail addresses: haiyangyu.cup@139.com (H.-Y. Yu), petroyang@163.com (Y. Wang).

https://doi.org/10.1016/j.petsci.2025.01.001

applied all over the world (Skauge et al., 2020; Du et al., 2021; Xiao et al., 2023). However, chemicals are requisite to generate foam, which will increase costs, and chemical absorption on rock surfaces also brings environmental risks (Belhaj et al., 2020).

Koide and Xue (2009) developed non-chemical microbubbles (MB) for CO_2-EOR and carbon sequestration, which is a low-cost, environmentally friendly technology that does not require any chemical agents. The main difference between MB and conventional foam is that MB is a foam system with spherical gas bubbles with a diameter on the order of tens of micrometers, while conventional foam has a semi-geometrical structure, which is often larger than 100 μm. The structure of MB brings several unique properties, including higher mass transfer rate (Sebba, 1971), higher ζ potential (Yoon and Yordan, 1986; Hasegawa et al., 2008), and better injectivity in low permeability reservoirs (Telmadarreie et al., 2016). These properties make MB a promising technology for EOR and carbon sequestration (Jiang et al., 2019). To reveal the EOR mechanism of CO_2 MB, many scholars have conducted experimental and numerical simulation studies. Xue et al. (2011) produced MB by ceramic membrane method and investigated the migration characteristics and EOR performance of MB using X-ray computer tomography (CT). Their findings demonstrated that MB effectively delayed CO_2 breakthrough and significantly increased sweep efficiency (Xue et al., 2014). Shi et al. (2016) evaluated the EOR performance of chemical-assisted MB and compared it with surfactant flooding. The authors observed that the oil recovery with MB was 6.5% higher than that achieved with surfactant flooding. Telmadarreir et al. (2016) examined the EOR performance of CO_2 MB for heavy oil recovery in a heterogeneous micro model. The author revealed that MB can increase oil recovery by improving sweep efficiency and causing oil emulsification. Zhai et al. (2020) investigated the migration characteristics of CO_2 MB, without the presence of oil, in Berea sandstone, using X-ray CT. The author reported that MB has better sweep efficiency than continuous gas injection, leading to improved pore space utilization and ultimately enhancing CO_2 storage capacity. Wang et al. (2023) studied the carbon sequestration and EOR mechanisms of CO_2 MB in sandpacks (permeability: from 7.8×10^{-3} to 22.25×10^{-3} μm^2) using nuclear magnetic resonance (NMR) scanning. It was found that MB increased CO_2 storage efficiency and oil recovery by 5.1% and 9.0%, respectively.

Although earlier research has demonstrated the potential of CO_2 MB in enhanced oil recovery and carbon sequestration, there are still gaps in the existing literature. For instance, the EOR mechanism of microbubbles in low permeability reservoirs and heterogeneous reservoirs has not been thoroughly investigated from a microscopic perspective. Additionally, the influence of MB injection on pore structure remains unexplored. Therefore, it is imperative to gain insights into residual oil saturation and the associated mechanisms during MB injection. To address these knowledge gaps, in this study, the NMR method was introduced to reveal the EOR mechanism of MB in low permeability reservoirs. NMR technology can capture signals of fluid migration during core flooding experiments, which is a powerful tool for quantified EOR mechanism studies (Qian et al., 2019; Li Y. et al., 2020; Li et al., 2022). Furthermore, the statistical analysis of the pore utilization during MB EOR was carried out. Finally, the impact of MB injection on the pore structure was revealed. The results of this study provide a further understanding of pore-level EOR mechanisms of CO_2 MB in low permeability reservoirs.

2. Experimental

2.1. Experimental materials

Fluid. Crude oil was taken from the Shengli Oilfield, China, and dehydrated before properties tests. At ambient conditions, the viscosity of the crude oil is 2.02 mPa s and the density is 868 kg/m^3. Then, the composition of the cured oil was revealed by gas chromatography, the results are shown in Fig. 1. The composition of a typical formation brine used is listed in Table 1. D_2O (purity > 99.9%, Ailan, Co. Ltd., China) was used to shield hydrogen signals and as base fluid in coreflood experiments. Industrially CO_2 (purity > 99.999%) was provided by Tianhao Gas Co., Ltd, China.

Cores. Sandstone core plugs used were sampled from the Shengli Oilfield, China, with a length of 7 cm and a diameter of 2.5 cm. Before experiments, all core plugs were cleaned with petroleum ether for 5 days and dried at 100 °C for 2 days to evaporate water. The petrophysical properties (porosity and permeability) were then measured using a steady state gas permeability meter and a porosity meter based on Boyle's law, respectively. The results are shown in Table 2.

2.2. Microbubble generation

A MB generator featuring a ceramics membrane (30 mm in diameter, 5 mm thick) was utilized to effectively produce uniform CO_2 MB. The schematic diagram of the MB generator and the process of bubble generation are depicted in Fig. 2. In MB generation, firstly, the brine is injected into the generator to form a continuous phase and expel any air in the pipeline. Secondly, the CO_2 and brine are pumped into the generator simultaneously. The continuous gases will be tearing by the capillary forces and the flowing liquid. Consequently, the CO_2 will transform into MB after flowing through the ceramic membrane. This MB generation method utilizes the porous media technique of MB generation (Parmar and Majumder, 2013; Liu et al., 2021; Xie et al., 2021; Jia et al., 2024a, 2024b), which involves injecting a gas–liquid mixture through a porous media to generate MB. The gas–liquid ratio of MB can be easily controlled by altering the flow rate of CO_2 and brine. The size of the MB is

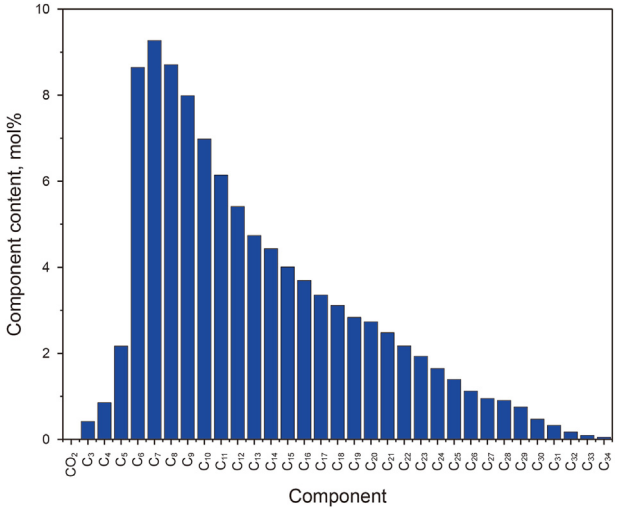

Fig. 1. Composition of crude oil at 25 °C.

Table 1
The brine composition.

Composition, mg/L				Salinity, mg/L
Na^+	K^+	Ca^{2+}	Cl^-	
1388	1537	68	3654	7086

Table 2
Properties of the sandstone cores.

Core#	Permeability, 10^{-3} μm^2	Standard deviation of permeability	Porosity, %	Standard deviation of porosity	Length, cm	Diameter, cm
1	9.53	0.0338	16.12	0.014	7.00	2.52
2	9.51	0.0335	16.25	0.013	7.02	2.52
3	2.17	0.0316	14.31	0.013	7.00	2.52
4	2.23	0.0310	14.35	0.019	7.02	2.52
5	9.45	0.0353	16.46	0.015	7.00	2.52
6	2.30	0.0332	14.23	0.018	7.02	2.52
7	9.47	0.0305	16.43	0.017	7.00	2.52
8	2.33	0.0321	14.26	0.018	7.02	2.52
9	9.52	0.0320	16.23	0.015	7.00	2.52

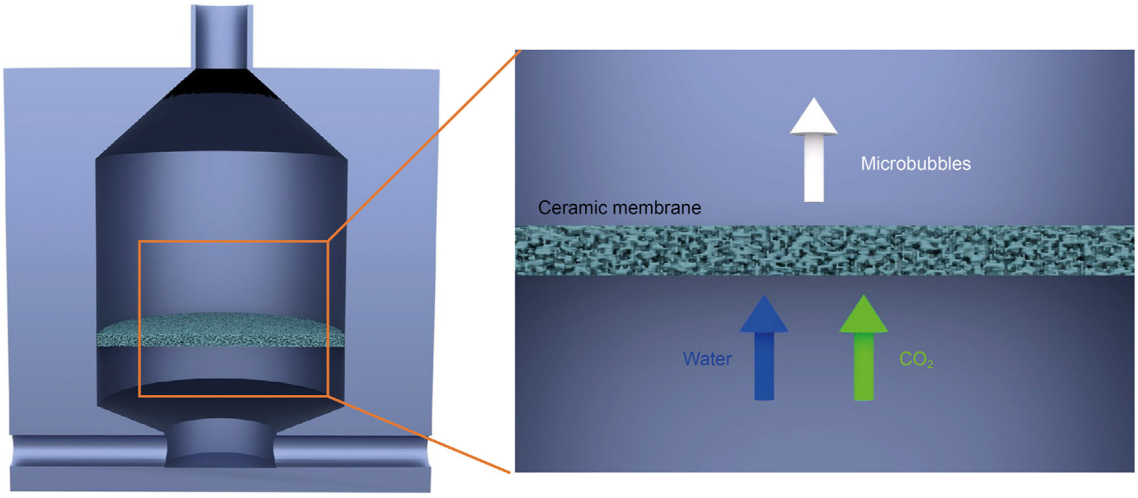

Fig. 2. The schematic diagram of the MB generator.

controlled by the average pore size of the membrane. In this study, the ceramic membrane with an average pore size of 4 μm was utilized.

2.3. Experimental setup

The NMR core displacement analysis system was employed. As illustrated in Fig. 3, the experimental setup mainly consisted of a NMR measurement device, a coreflood system, and a data logging system. The NMR measurement system (MacroMR12-150H-VTHP, Suzhou Niumag Analytical Instrument Corp., China) was used to determine the T_2 spectra. The NMR spectrometer was equipped with a permanent magnet operating at a magnetic field strength of 0.3±0.05 T, and a resonance frequency of 12.446 MHz. The CPMG sequence, with an echo number of 12,000 and scanning number of 64 was used in this study. The coreflood system consisted of a syringe pump (Model 500D, Teledyne Isco. Inc., USA), two high-pressure vessels containing brine and CO_2, a mass flow controller, a back pressure regulator (Model 93, Xiongchuang Inc., China) for maintaining the outlet pressure and the data logging system consisted of a differential pressure sensor and a computer. The measuring tube at the outlet was used to measure the volume of oil and water in effluents. The injection pump was operated at constant volume mode to control the injection of CO_2 and brine.

2.4. Experimental procedures

Mobility reduction factor examination. Before conducting core flooding experiments, the mobility reduction factors of MB at different gas–liquid ratios were determined. The experiments were performed under Shengli Oilfield's formation conditions (10 MPa, 40 °C). The mobility reduction factors (F_{MR}) is defined as a ratio of pressure drop with MB to that without MB at the same total superficial velocity:

$$F_{MR} = \frac{\Delta P_{MB}}{\Delta P_{water}} \quad (1)$$

where F_{MR} is the mobility reduction factor; ΔP_{MB} and ΔP_{water} denote the pressure drop along the core sample with MB and without MB, respectively. The experimental conditions used in F_{MR} examination are the same as in EOR experiments.

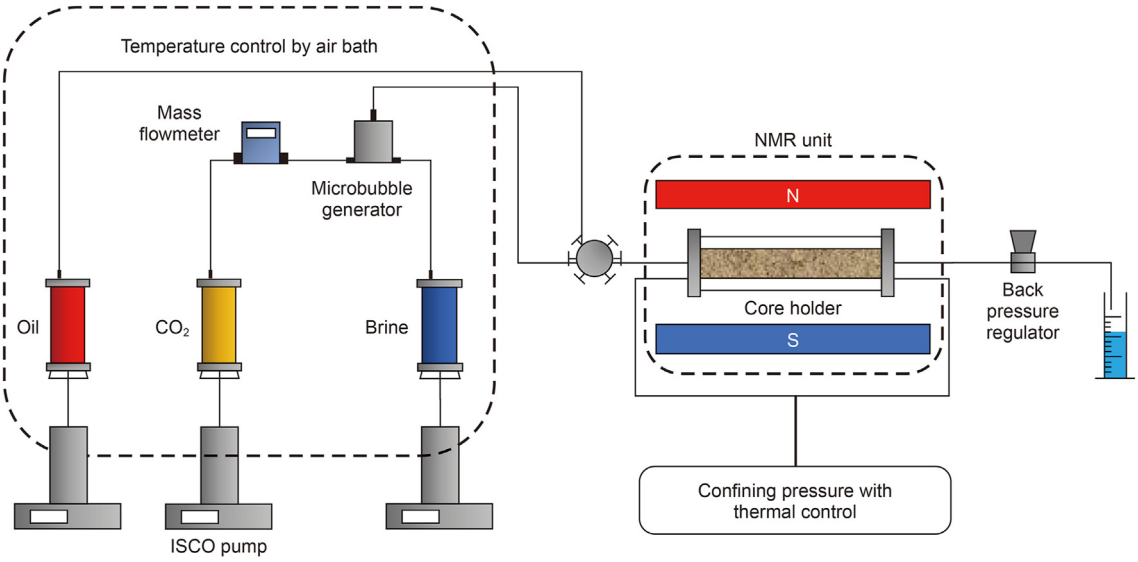

Fig. 3. Schematic of NMR microbubble displacement experiment.

(1) The fluids were heated at 40 °C until the temperature in the oven was stabilized.
(2) The back pressure of 10 MPa was applied at the back pressure regulator. The core sample was saturated with brine.
(3) Water injection stage: the brine was injected into the core sample until the ΔP_{water} was stabilized.
(4) MB injection stage: MB was injected into the core sample until the ΔP_{MB} was stabilized.

NMR core flooding. Before NMR core flooding experiments, the core was tested for iron substance to avoid interfering with the magnetic field. The experiments were performed under the Shengli Oilfield's formation conditions (10 MPa, 40 °C). The experimental procedures can be summarized as follows:

(1) The fluids were heated at 40 °C until the temperature in the oven was stabilized.
(2) The back pressure of 10 MPa was applied at the back pressure regulator. The core sample was saturated with brine. Then, the core samples were saturated with oil to establish a residual water state.
(3) NMR scanning was performed and the initial T_2 spectrum of the core sample at saturated oil state was obtained.
(4) Water flooding (WF) stage: brine was injected into the core sample until there was no more oil coming out.
(5) Tertiary flooding stage: MB were injected into the core sample for 1 pore volume (PV).
(6) Subsequent water flooding stage: brine was injected into the core until there was no more oil coming out. The oil recovery ratio and pressure drop along the core holder were calculated and metered during the flooding process, respectively.
(7) During the experiment, the NMR scanning was performed to get the T_2 spectrum at different stages.

Due to limitations with the NMR units, only one core holder could be scanned at a time during the parallel coreflood experiments. As a result, the parallel core flooding experiments were conducted twice. In the first round, the NMR scans were performed on the high permeability core, and in the second round, the NMR scans were conducted on the low permeability core. To ensure the consistency and reliability of the results, core samples with similar permeability, porosity, and T_2 spectra were carefully selected. This approach helps to minimize the variability in the experimental data and ensures that the observed effects are more directly attributable to the MB EOR process being investigated.

Change of pore structure by MB. Prior to conducting experiments, the permeability and the porosity of the core samples were determined. The core samples were then saturated with formation brine (base fluid: H_2O), and MB was injected into the core samples for 1 PV (39.0 min). Subsequently, post water flooding was conducted until the pressure drop along the core samples stabilized. NMR scans were performed to collect T_2 spectra data.

2.5. Conversation between T_2 and pore radius

Two types of relaxation time can be determined in NMR tests: longitudinal relaxation time (T_1) and transverse relaxation time (T_2). T_2 is positively correlated with the substances containing hydrogen atoms in the porous media. Therefore, T_2 can be used to characterize the fluid distribution. T_2 comprises three different relaxation mechanisms: surface relaxation time ($T_{2,surface}$), bulk relaxation time ($T_{2,bulk}$) and diffusion relaxation time ($T_{2,diffsusion}$)

$$\frac{1}{T_2}=\frac{1}{T_{2,surface}}+\frac{1}{T_{2,bulk}}+\frac{1}{T_{2,diffsusion}} \tag{2}$$

Previous studies have reported that $T_{2,bulk}$ and $T_{2,diffsusion}$ can be neglected while $T_{2,surface}$ contributes more in T_2 spectrum (Connolly et al., 2019; Wei et al., 2019; Li S. et al., 2020; Tang et al., 2023). Thus, Eq. (1) can be reduced to

$$\frac{1}{T_2}=\frac{1}{T_{2,surface}}=\rho_2\left(\frac{S}{V}\right)_{pore} \tag{3}$$

where ρ_2 is the surface relaxivity; S/V is the ratio between the internal surface area to the pore volume. Letting $S/V = F_s/R$, Eq. (2) can be expressed as

$$\frac{1}{T_2}=\frac{1}{T_{2,surface}}=\rho_2\frac{F_s}{R} \tag{4}$$

where F_s is the shape factor of the pore; R is the pore radius. In the

NMR test, the ρ_2 and F_s can be assumed to be constant values. Therefore, Eq. (3) can be expressed as

$$T_2 = \frac{R}{\rho_2 F_s} \tag{5}$$

Previous studies show that the pore radius is a power function of T_2 (Li et al., 2015). Letting $C = \rho_2 F_s$, the conversation between T_2 and pore radius is

$$R = C T_2^{\,n} \tag{6}$$

where coefficients C and n are 1.1767 and 0.6506, respectively, based on mercury intrusion porosimetry (MIP) data.

3. Results and discussion

3.1. Gas–liquid ratio of MB

The conformance control of MB is influenced by the gas–liquid ratio during MB generation. Therefore, before core flooding experiments, it is essential to determine the mobility reduction factor of MB under various gas–liquid ratios. The gas–liquid ratio is the volume ratio of gas and liquid phases under reservoir conditions. As shown in Fig. 4, the mobility reduction factor of MB gradually increased with the increase of the gas–liquid ratio, and the peak value of mobility reduction factor was 3.79, with a gas–liquid ratio of 1. The conformance control of MB was not pronounced until the gas–liquid ratio reached 1. However, the mobility reduction factor gradually decreased when the gas–liquid ratio exceeded 1. The mobility reduction factor decreased to 1.54 with a gas–liquid ratio of 5. This behavior can be attributed to the increase in the gas phase, which increases the bubble diameter. This, in turn, results in a mismatch between the bubble diameter and the pore radius, leading to poor conformance control performance. Our previous study observed that MB with the gas–liquid ratio of 1:1 has an average bubble diameter of 34 μm (Jia et al., 2023). Moreover, as the gas–liquid ratio increased, the MB became drier, and more bubbles coalesced with each other, which was unfavorable for conformance control. Because the MB generation method used in this study does not include surfactants and gels to enhance the strength of the liquid film between the bubbles, the stability of MB is more susceptible to damage under high gas–liquid ratio conditions. Therefore, MB with a gas–liquid ratio of 1 was selected in EOR experiments.

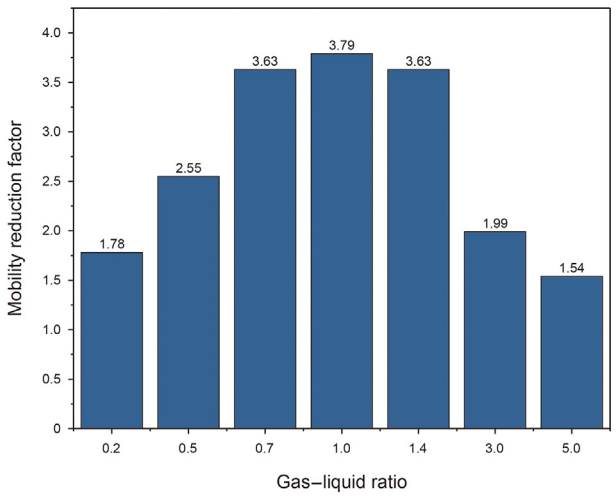

Fig. 4. Mobility reduction factor of MB as the function of gas–liquid ratio.

3.2. EOR mechanisms of MB

3.2.1. MB EOR in homogeneous porous media

To reveal the EOR mechanism of CO_2 MB, CO_2 flooding and CO_2 MB flooding were performed in core #1 and core #2, respectively. The oil recovery, along with the pressure, during CO_2 flooding are depicted in Fig. 5(a). It can be found that the pressure drop first increased and then decreased gradually during the water injection stage. The oil recovery after WF was 54.37% of the original oil in place (OOIP). After WF, CO_2 flooding was performed to enhance oil recovery. The gas breakthrough occurred at 0.4 PV, after which the oil recovery increased slowly and the pressure drop also decreased. The final oil recovery for the CO_2 flooding was 64.38% of OOIP, with an incremental oil recovery of 10.01% of OOIP. Fig. 5(b) depicts the pressure drop and oil recovery during CO_2 MB injection. As shown, there was a significant increase in the pressure drop curve at the beginning of the MB injection stage. The peak value of pressure drop during the MB stage was 1.78 MPa, and the gas breakthrough occurred at 0.7 PV. The increase in pressure drops indicates the increase in flow resistance, which highlights the conformance control of MB. The oil recovery of MB injection was 68.15% of OOIP, with an incremental oil recovery of 13.49% of OOIP.

To further analyze the EOR mechanisms of MB from the microscope view, the NMR tests were conducted during core flooding experiments. Fig. 6(a) shows the distribution of oil during CO_2 flooding in core #1. In Fig. 6, the horizontal axis is the pore radius converted by T_2 and the vertical axis is the signal amplitude representing the volume of fluid with a hydrogen nucleus, which is oil in the experiments. The oil recovery can be determined by calculating the area difference between two measurements (Mitchell et al., 2013; Wei et al., 2019; Yu et al., 2021b; Gong et al., 2022; Siavashi et al., 2022; Zhang et al., 2022). To further characterize the distribution of oil, the pores radius was divided into 3 regimes: 0.01–1 μm (small pores), 1–10 μm (median pores), > 10 μm (large pores). At the initial state, the oil was distributed with a pore radius interval ranging from 0.05 to 33.97 μm. After CO_2 flooding, as shown in Table 3, the incremental oil recovery in the pore interval of > 10 μm was higher than in other pore intervals, suggesting that large pores contributed more to the oil recovery. Fig. 6(a) shows the distribution of oil after CO_2 flooding in core #1. In CO_2 flooding, due to the lack of conformance control, CO_2 would break through the core sample through large pores, leaving the small pores poorly swept. The oil recovery in small pores was increased to 10.36% after CO_2 flooding. Fig. 6(b) shows the distribution of oil after CO_2 MB flooding in core #2, as shown, the oil in all pore regimes decreased. After injecting 1 PV of MB, the small pores contributed more significantly to the final oil recovery. The oil recovery in small pores reached to 46.33%. The increase in pressure drops due to the "Jamine effect" during MB flooding led to increased flow resistance in the large pores (Li Y. et al., 2020). Consequently, MB was diverted into the small pores, resulting in higher sweep efficiency and higher oil recovery.

Fig. 7 shows CO_2 and MB EOR performance in core #3 and core 4#, respectively. As shown, CO_2 flooding and CO_2 MB flooding had different performances. Regarding CO_2 flooding, the incremental oil recovery was only 8.77% of OOIP and the final oil recovery reached 32.40% of OOIP. In MB flooding, the incremental oil recovery was 22.80% of OOIP and the final oil recovery was 44.60% of OOIP.

As Fig. 8 shows, at the initial state, the oil was mainly distributed with a pore radius interval ranging from 0.049 to 44.61 μm. Notably, the NMR tests at oil saturated state revealed the presence of oil in 121.09–250.36 μm in core #3 and 84.22–145.21 μm in core #4, indicating the microheterogeneity within the core samples. As shown, the small pores barely contributed to the final oil recovery (Table 4), which indicates that the most of residual oil area was not

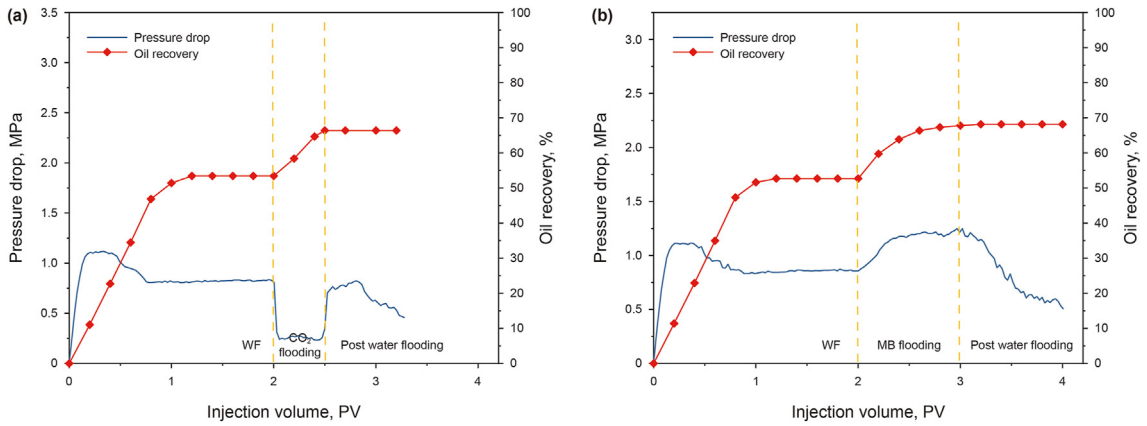

Fig. 5. Pressure drops and oil recovery in high permeability cores: (**a**) core #1, CO_2 flooding; (**b**) core #2, MB flooding.

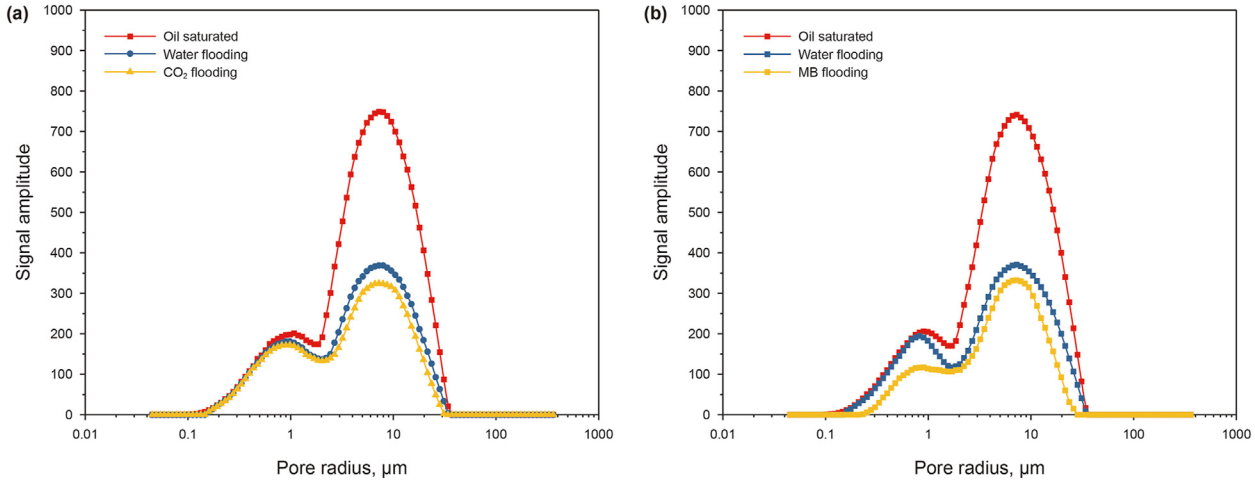

Fig. 6. The distribution of oil during EOR in high permeability cores: (**a**) core #1, CO_2 flooding; (**b**) core #2, MB flooding.

Table 3
Oil recovery in different pore regimes of high permeability cores.

Stage	Oil recovery in different pore regimes, %		
	0.01–1 μm	1–10 μm	> 10 μm
WF	6.87	49.50	53.87
CO_2 + post WF	10.36	55.75	66.36
WF	5.75	49.20	50.00
MB + post WF	46.33	55.68	74.19

swept by CO_2. Due to the microheterogeneity of the core sample, gas channeled at an early stage of flooding and could not enter the small pores, resulting in low sweep efficiency and oil recovery. For MB flooding, the results show that the residual oil in all pore radius regimes were swept (Fig. 8(b)). After the MB flooding, the oil recovery in small pores, median pores and large pores were increased to 53.21%, 38.24%, and 47.40%, respectively. This was due to the increase in pressure drops along the core sample, which promoted microbubbles to enter the small pores. Overall, after MB flooding, the signal amplitude was decreased in both small pores and large pores regimes, demonstrating that MB has superior conformance control ability which can improve sweep efficiency, especially in core with microheterogeneity.

3.2.2. MB EOR in heterogeneous porous media

To reveal MB EOR performance and mechanisms in heterogeneous reservoirs, the parallel coreflood experiments with NMR monitoring were conducted. The oil recovery curve is depicted in Fig. 9. As shown in Fig. 9, in run 1 and run 2, the oil recovery in the high permeability core and low permeability core both increased as water injection proceeded. As water broke through the high permeability core, the oil recovery in the low permeability core barely increased. In run 1, after water injection, the oil recovery in the high permeability core and low permeability core were 54.11% and 15.20% of OOIP, respectively. Due to reservoir heterogeneity, the oil recovery in low permeability core was lower than that in the single coreflood experiment. As MB was injected, the oil recovery in both core samples increased significantly. The incremental oil recovery in the high permeability core and low permeability core were 15.73% and 16.07% of OOIP, respectively. The total oil recovery was increased from 38.70% to 54.57% of OOIP. Similarly, in run 2, the oil recovery after water injection in the high permeability core and low permeability core were 53.65% and 14.98% of OOIP, respectively. The incremental oil recovery by MB injection in high permeability core and low permeability core were 16.67% and 16.85% of OOIP, respectively. The total oil recovery was increased from 38.34% to 55.08% of OOIP. The results in run 2 were close to those in run 1, which demonstrates the feasibility of comparing the two parallel coreflood experiments.

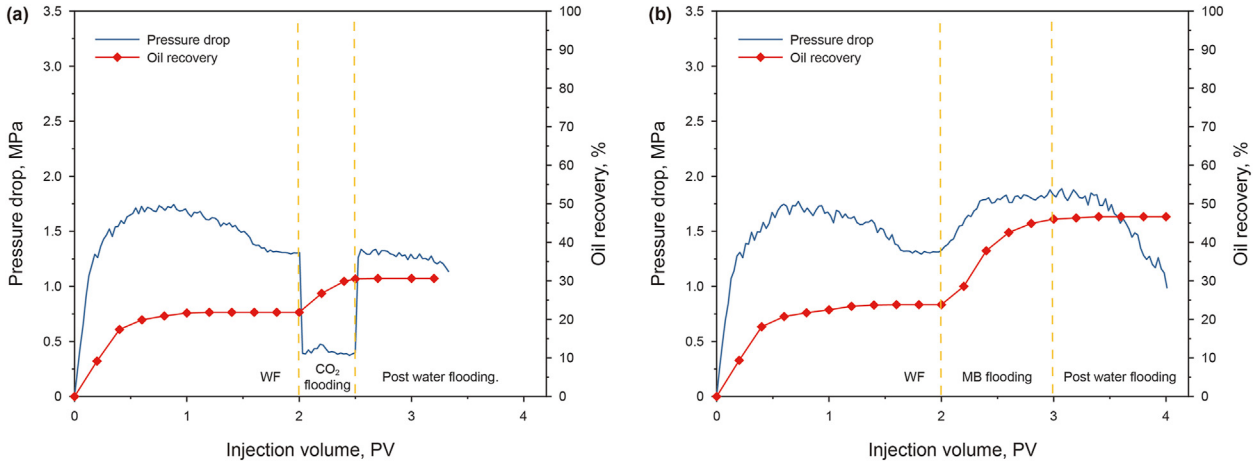

Fig. 7. Pressure drops and oil recovery in low permeability cores: (**a**) core #3, CO_2 flooding; (**b**) core #4, MB flooding.

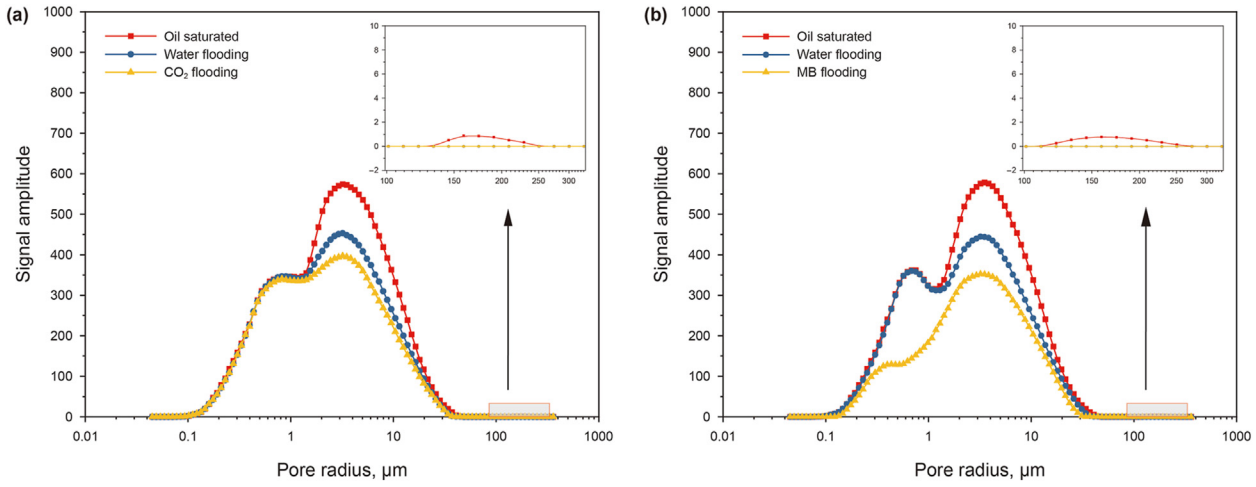

Fig. 8. Distribution of oil during EOR in low permeability cores: (**a**) core #3, CO_2 flooding; (**b**) core #4, MB flooding.

Table 4
Incremental oil recovery in different pore regimes of low permeability cores.

Stage	Oil recovery in different pore regimes, %		
	0.01–1 μm	1–10 μm	> 10 μm
WF	0.76	22.36	26.99
CO_2 + post WF	2.26	31.53	35.51
WF	1.35	23.48	27.53
MB + post WF	53.21	38.24	47.40

As shown in Fig. 10(a), the distribution of oil in the high permeability core was similar to those in a single coreflood scenario, where the large pores primarily contributed to the oil recovery during water flooding. However, the low permeability core was poorly flooded due to the reservoir heterogeneity (Fig. 10(b)). As the pore interval analysis of low permeability core sample shows (Table 5), 13.35% of the oil was recovered in large pores, while the oil recovery in small pores was only 1.46%. After MB flooding, the oil recovery in large pores and small pores was 29.31% and 42.20%. Notably, the oil recovery of the high permeability core in parallel core flooding was higher than that in single core flooding experiments. This discrepancy can be attributed to permeability contrast, which results in more injected water flowing into the high

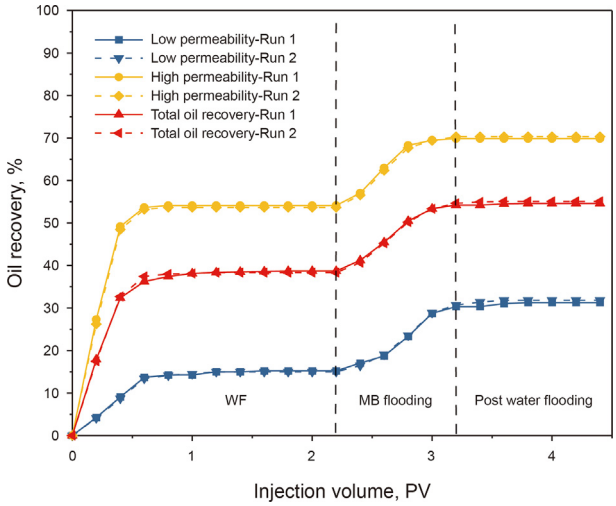

Fig. 9. Oil recovery in parallel coreflood experiment.

permeability core, thereby leading to higher oil recovery after both WF and MB flooding stages. In contrast, for the low permeability

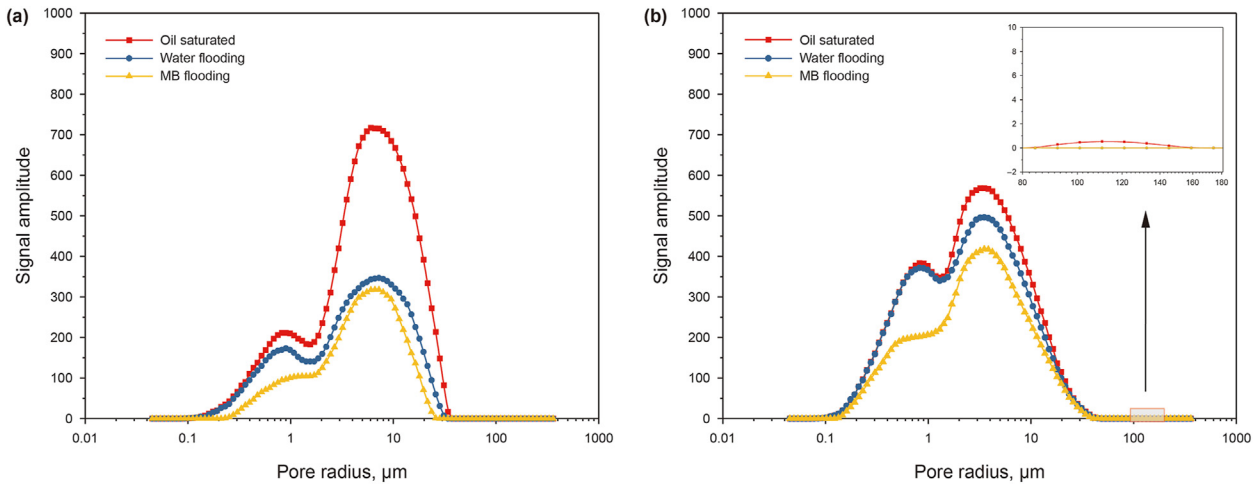

Fig. 10. The distribution of oil in parallel MB flooding experiment: (**a**) high permeability core; (**b**) low permeability core.

Table 5
Oil recovery in different pore regimes.

Core #	Stage	Oil recovery in different pore regimes, %		
		0.01–1 μm	1–10 μm	> 10 μm
5	WF	16.89	49.26	59.00
	MB + post WF	58.94	55.02	77.78
8	WF	1.46	13.07	13.35
	MB + post WF	42.20	29.49	29.31

core sample, it took time for MB to divert fluid into the low permeability core sample. Consequently, the oil recovery in the low permeability core sample was lower than that in single core flooding experiments. In general, the results highlight the conformance control abilities of MB in heterogeneous reservoirs.

3.2.3. EOR mechanisms and advantages

Based on the findings of this study, Fig. 11 presents a schematic diagram illustrating the EOR mechanism of MB. After WF, there are three types of residual oil (Ma et al., 2012; Li Y. et al., 2020): (1) oil droplets absorbed on the surface of the pore, (2) oil trapped by capillary forces in the pore channel, and (3) oil in unswept low permeability zones. It is challenging to recover these proportions of crude oil through continued WF alone. Upon injecting CO_2 MB into the core, due to the original brine in the core sample was not saturated by CO_2, a portion of the CO_2 gas bubbles will dissolve into the water, forming carbonate water (CW) (Jia et al., 2023). Subsequently, CW will come into contact with the oil ahead of the MB. As the solubility of CO_2 in oil is higher than that in water (Mosavat, 2014; Han et al., 2024), the dissolved CO_2 will gradually transfer into the oil droplets, reducing the viscosity of the crude oil and the interfacial tension between oil and water. And the oil droplets will swell upon contact with CO_2, making them easier to flow. As MB flow through the pore surface, the residual oil will be recovered. Moreover, because MB significantly increases the flow resistance, the residual oil in trapped pore channels and low permeability zones will also be swept, leading to higher oil recovery.

The CO_2 utilization factor is defined as mass or volume of CO_2 required to produce one incremental barrel of oil (kg CO_2/bbl oil or Mscf CO_2/bbl oil). The results show that MB has better CO_2 utilization factors than CO_2 flooding, both in high-permeability cores and low-permeability cores (Table 6). The results suggest that MB has higher CO_2 utilization efficiency, which is critical in CO_2 EOR and CCUS.

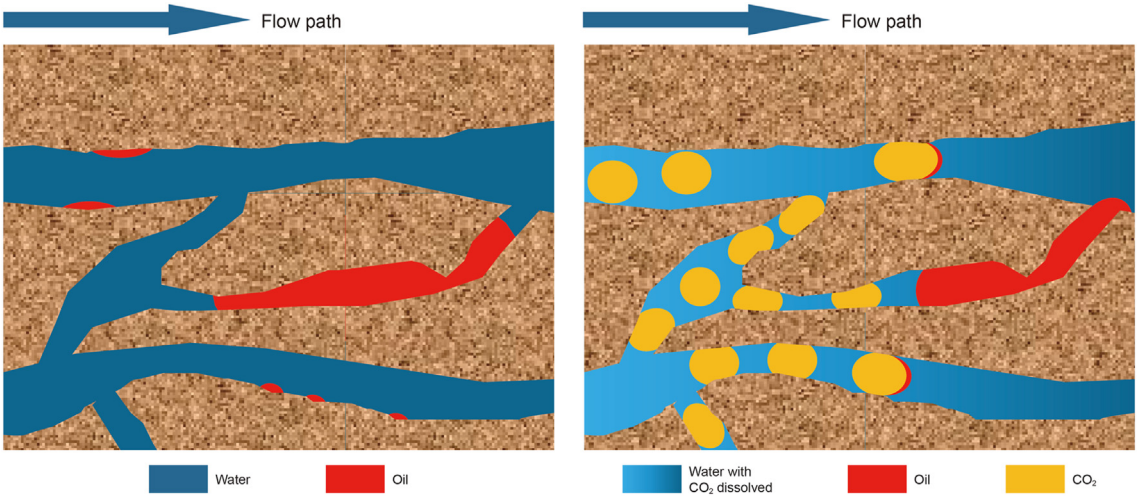

Fig. 11. EOR mechanisms of MB.

Table 6
CO_2 utilization factors.

Core #	Permeability, 10^{-3} μm^2	Experimental scheme	CO_2 utilization factor, Mscf/bbl
1	9.53	WF + CO_2	1.85
2	9.51	WF + MB	1.41
3	2.17	WF + CO_2	3.12
4	2.23	WF + MB	1.31

3.3. Change of pore structure by MB

Previous studies have revealed that minerals in sandstone reservoirs are mainly carbonate mineral (Wang et al., 2022), which can be dissolved by carbonic acid created by CO_2 and water. Common minerals in sandstone reservoirs are dolomite, calcite, and silicate minerals of feldspar, including potassium feldspar, sodium feldspar, and calcium feldspar. As discussed earlier, the CO_2 bubbles will dissolve into the brine immediately after generation, meaning that microbubbles consist of CW and CO_2 bubbles. Compared to CO_2 flooding and WAG, MB is more likely to trigger mineral reactions in the reservoirs because the CW is already saturated with CO_2, which takes less time for CO_2 to dissolve into the water.

The impact of MB flooding on pore structure was investigated using core #9. Table 7 demonstrates the change of permeability and porosity by MB flooding. The permeability and the porosity of the core sample were increased by 17.54% and 0.31%, respectively. It can be observed that MB can significantly improve the petrophysical properties of core samples, particularly in permeability. Fig. 12 illustrates the pore distribution of the core sample before and after MB flooding. It can be found that there was a significant increase in the right peak at 6.05 μm, which demonstrates the increase of pore space by MB. As pore radius interval analysis showed (Table 8), the pore space in different intervals was increased with varying degrees. The small pore regime exhibited the highest increments, suggesting that MB can dissolve minerals in the core sample, enlarging the diameter of the pores and throats, particularly in the small pore and throat regimes. This enhancement is favorable for improving the petrophysical properties of the reservoir.

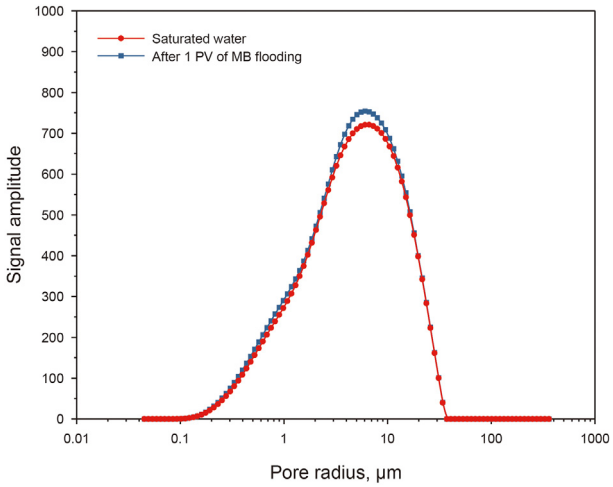

Fig. 12. Effect of MB on pore structure.

Table 8
Change of pore space in different regimes.

Stage	Chang of pore space, %		
	0.01–1 μm	1–10 μm	> 10 μm
After MB treated	7.78	3.86	1.56

4. Conclusions

In this study, laboratory investigations were conducted to understand the EOR mechanisms of non-chemical CO_2 MB. The NMR scans were performed to acquire MB dynamics in heterogeneous reservoirs. Moreover, the impact of MB flooding on pore structure was also revealed. The major conclusions drawn from this study are summarized as follows:

(1) The NMR analysis shows that MB has superior conformance control abilities that can recover residual oil in small pores. MB can adjust flows in different zones of a micro heterogeneous media, and improve the sweeping efficiency significantly. Compared to CO_2 flooding, MB yielded higher oil recovery, which was 68.15% and 46.63% of OOIP in high permeability and low permeability core samples, respectively.

(2) Parallel coreflood experiment demonstrates that the injection of MB can effectively improve the sweep efficiency in the low permeability heterogeneous porous media. The NMR analysis shows that in the low permeability core sample, the oil recovery in the small pore regime was significantly increased. The total oil recovery was increased from 38.70% to 54.57% of OOIP by MB in run 1. MB exhibited good conformance control performance in the heterogeneous reservoir.

(3) Under experimental conditions in this study, MB can significantly improve the pore structure of low permeability reservoirs. Under experimental conditions in this study, the permeability and porosity of the core sample were increased by 17.54% and 0.31%, respectively, which is beneficial for oil production. Additionally, these findings underscore the carbon sequestration potential of MB due to the interactions between CO_2 and minerals, which affect injectivity and ultimately lead to higher carbon sequestration efficiency.

Table 7
Petrophysics properties of the core sample.

Stage	Permeability, 10^{-3} μm^2	Standard deviation of permeability	Porosity, %	Standard deviation of porosity
Initial state	9.52	0.032	16.23	0.015
After 1 PV MB + post WF	11.14	0.037	16.28	0.013

CRediT authorship contribution statement

Hao-Wei Jia: Validation, Methodology, Investigation. **Hai-Yang Yu:** Writing – review & editing, Supervision. **Rui Ma:** Validation, Investigation, Data curation. **Peng Song:** Resources. **Zhou Yuan:** Resources, Funding acquisition. **Jing-Pu Zhang:** Investigation. **Tao Huang:** Investigation. **Jun Lu:** Validation. **Yang Wang:** Writing – review & editing, Supervision.

Declaration of competing interest

The authors declare that they have no known competing financial interests or personal relationships that could have appeared to influence the work reported in this paper.

Acknowledgments

This work was financially supported by the National Natural Science Foundation of China (52074317), the PetroChina Group Major Special Project (2021ZZ01-03), and the National Key Research and Development Program (2023YFF0614100).

References

Ajayi, T., Gomes, J.S., Bera, A., 2019. A review of CO_2 storage in geological formations emphasizing modeling, monitoring and capacity estimation approaches. Petrol. Sci. 16, 1028–1063. https://doi.org/10.1007/s12182-019-0340-8.

Belhaj, A.F., Elraies, K.A., Mahmood, S.M., Zulkifli, N.N., Akbari, S., Hussien, O.S., 2020. The effect of surfactant concentration, salinity, temperature, and pH on surfactant adsorption for chemical enhanced oil recovery: a review. J. Pet. Explor. Prod. Technol. 10, 125–137. https://doi.org/10.1007/s13202-019-0685-y.

Connolly, P.R., Vogt, S.J., Mahmoud, M., Ng, C.N., May, E.F., Johns, M.L., 2019. Capillary trapping of CO_2 in sandstone using low field NMR relaxometry. Water Resour. Res. 55 (12), 10466–10478. https://doi.org/10.1029/2019WR026294.

Du, D., Zhao, D., Li, Y., Wang, F., Li, J., 2021. Parameter calibration of the stochastic bubble population balance model for predicting NP-stabilized foam flow characteristics in porous media. Colloids Surf. A Physicochem. Eng. Asp. 614, 126180. https://doi.org/10.1016/j.colsurfa.2021.126180.

Fang, T., Wang, M., Gao, Y., Zhang, Y., Yan, Y., Zhang, J., 2019. Enhanced oil recovery with CO_2/N_2 slug in low permeability reservoir: molecular dynamics simulation. Chem. Eng. Sci. 197, 204–211. https://doi.org/10.1016/j.ces.2018.12.016.

Gong, H., Zhang, H., Lv, W., Xu, L., Li, Z., Dong, M., 2022. Effects of Kerogen on the flow and EOR performance of oil in shale cores during CO_2 flooding process investigated by NMR technology. SPE J. 27 (4), 2244–2256. https://doi.org/10.2118/209581-PA.

Han, X., Yu, H., Tang, H., Song, P., Huang, T., Liu, C., Wang, Y., 2024. Investigation on oil recovery and countercurrent imbibition distance coupling carbonated water with surfactant in shale oil reservoirs. Fuel 374, 132409. https://doi.org/10.1016/j.fuel.2024.132409.

Hasan, M.F., First, E.L., Boukouvala, F., Floudas, C.A., 2015. A multi-scale framework for CO_2 capture, utilization, and sequestration: CCUS and CCU. Comput. Chem. Eng. 81, 2–21. https://doi.org/10.1016/j.compchemeng.2015.04.034.

Hasegawa, H., Nagasaka, Y., Kataoka, H., 2008. Electrical potential of microbubble generated by shear flow in pipe with slits. Fluid Dynam. Res. 40 (7–8), 554–564. https://10.1016/j.fluiddyn.2007.12.007.

Hill, L.B., Li, X., Wei, N., 2020. CO_2-EOR in China: a comparative review. Int. J. Greenh. Gas Control 103, 103173. https://doi.org/10.1016/j.ijggc.2020.103173.

Jia, H., Yu, H., Wang, S., Shi, J., Xie, F., Wang, S., Lu, J., Wang, Y., Zhang, F., 2024a. Investigation of CO_2 microbubble assisted carbon sequestration and gravity-induced microbubble ripening in low permeability reservoirs. Appl. Energy 373, 123954. https://doi.org/10.1016/j.apenergy.2024.123954.

Jia, H., Yu, H., Xie, F., Yuan, Z., Xu, K., Wang, Y., 2023. Research on CO_2 microbubble dissolution kinetics and enhanced oil recovery mechanisms. Chin. J. Theor. Appl. Mech. 55 (3), 755–764.

Jia, H., Yu, H., Wang, T., Song, P., Song, J., Wang, Y., 2024b. Investigation of non-chemical CO_2 microbubbles for enhanced oil recovery and carbon sequestration in heterogeneous porous media. Geoenergy Sci. Eng. 242, 213229. https://doi.org/10.1016/j.geoen.2024.213229.

Jiang, L., Xue, Z., Park, H., 2019. Enhancement of CO_2 dissolution and sweep efficiency in saline aquifer by micro bubble CO_2 injection. Int. J. Heat Mass Tran. 138, 1211–1221. https://doi.org/10.1016/j.ijheatmasstransfer.2019.04.139.

Jiménez-de-la-Cuesta, D., Mauritsen, T., 2019. Emergent constraints on Earth's transient and equilibrium response to doubled CO_2 from post-1970s global warming. Nat. Geosci. 12 (11), 902–905. https://doi.org/10.1038/s41561-019-0463-y.

Kang, W., Zhou, B., Issakhov, M., Gabdullin, M., 2022. Advances in enhanced oil recovery technologies for low permeability reservoirs. Petrol. Sci. 19 (4), 1622–1640. https://doi.org/10.1016/j.petsci.2022.06.010.

Koide, H., Xue, Z., 2009. Carbon microbubbles sequestration: a novel technology for stable underground emplacement of greenhouse gases into wide variety of saline aquifers, fractured rocks and tight reservoirs. Energy Proc. 1 (1), 3655–3662. https://10.1016/j.egypro.2009.02.162.

Li, A., Ren, X., Wang, G., Wang, Y.-z., Jiang, K.-l., 2015. Characterization of pore structure of low permeability reservoirs using a nuclear magnetic resonance method. J. China Univ. Petrol. (Edition of Natural Science) 39 (6), 92–98.

Li, S., Wang, Q., Zhang, K., Li, Z., 2020. Monitoring of CO_2 and CO_2 oil-based foam flooding processes in fractured low-permeability cores using nuclear magnetic resonance (NMR). Fuel 263, 116648. https://doi.org/10.1016/j.fuel.2019.116648.

Li, X., Chen, X., Xu, Z., Pu, C., 2022. A novel foam flooding for enhanced oil recovery in fractured low-permeability reservoirs: performance evaluation and mechanism study. SPE J. 27 (4), 2408–2424. https://doi.org/10.2118/209623-PA.

Li, Y., Di, Q., Hua, S., Jia, X., Zhou, X., Wang, W., Chen, H., 2020. Visualization of foam migration characteristics and displacement mechanism in heterogeneous cores. Colloids Surf. A Physicochem. Eng. Asp. 607, 125336. https://doi.org/10.1016/j.colsurfa.2020.125336.

Liu, N., Chen, X., Ju, B., He, Y., Yang, Y., Brantson, E.T., Tian, Y., 2021. Microbubbles generation by an orifice spraying method in a water-gas dispersion flooding system for enhanced oil recovery. J. Petrol. Sci. Eng. 198, 108196. https://doi.org/10.1016/j.petrol.2020.108196.

Liu, Y., Hu, T., Rui, Z., Zhang, Z., Du, K., Yang, T., Dindoruk, B., Halfdan Stenby, E., Torabi, F., Afanasyev, A., 2023. An integrated framework for geothermal energy storage with CO_2 sequestration and utilization. Engineering 30, 121–130. https://doi.org/10.1016/j.eng.2022.12.010.

Liu, Y., Rui, Z., 2022. A storage-driven CO_2 EOR for a net-zero emission target. Engineering 18, 79–87. https://doi.org/10.1016/j.eng.2022.02.010.

Ma, K., Liontas, R., Conn, C.A., Hirasaki, G.J., Biswal, S.L., 2012. Visualization of improved sweep with foam in heterogeneous porous media using microfluidics. Soft Matter 8 (41), 10669–10675. https://doi.org/10.1039/C2SM25833A.

Mitchell, J., Staniland, J., Chassagne, R., Mogensen, K., Frank, S., Fordham, E.J., 2013. Mapping oil saturation distribution in a limestone plug with low-field magnetic resonance. J. Petrol. Sci. Eng. 108, 14–21. https://doi.org/10.1016/j.petrol.2013.04.008.

Mosavat, N., 2014. Utilization of Carbonated Water Injection (CWI) as a Means of Improved Oil Recovery in Light Oil Systems: Pore-Scale Mechanisms and Recovery Evaluation. Ph.D Dissertation. The University of Regina, Canada.

Parmar, R., Majumder, S.K., 2013. Microbubble generation and microbubble-aided transport process intensification—a state-of-the-art report. Chem. Eng. Process: Process Intensif. 64, 79–97. https://doi.org/10.1016/j.cep.2012.12.002.

Qi, S., Yu, H., Han, X., Xu, H., Liang, T., Jin, X., Qu, X., Du, Y., Xu, K., 2022a. Countercurrent imbibition in low-permeability porous media: non-diffusive behavior and implications in tight oil recovery. Petrol. Sci. 20 (1), 322–336. https://doi.org/10.1016/j.petsci.2022.10.022.

Qi, S., Yu, H., Xie, F., Hu, M., Lu, J., Wang, Y., 2022b. Experimental investigation on the CO_2 effective distance and CO_2-EOR storage for tight oil reservoir. Energy Fuel. 37 (1), 339–349. https://10.1021/acs.energyfuels.2c03544.

Qian, K., Yang, S., Dou, H.-e., Pang, J., Huang, Y., 2019. Formation damage due to asphaltene precipitation during CO_2 flooding processes with NMR technique. Oil Gas Sci. Technol. Revue d'IFP Energies nouvelles 74, 11. https://doi.org/10.2516/ogst/2018084.

Ren, B., Male, F., Duncan, I.J., 2022. Economic analysis of CCUS: accelerated development for CO_2 EOR and storage in residual oil zones under the context of 45Q tax credit. Appl. Energy 321, 119393. https://doi.org/10.1016/j.apenergy.2022.119393.

Sebba, F., 1971. Microfoams—an unexploited colloid system. J. Colloid Interface Sci. 35 (4), 643–646. https://doi.org/10.1016/0021-9797(71)90223-2.

Shi, S., Wang, Y., Li, Z., Chen, Q., Zhao, Z., 2016. Laboratory investigation of the factors impact on bubble size, pore blocking and enhanced oil recovery with aqueous Colloidal Gas Aphron. J. Pet. Explor. Prod. Technol. 6, 409–417. https://doi.org/10.1007/s13202-015-0193-7.

Siavashi, J., Najafi, A., Sharifi, M., Fahimpour, J., Shabani, M., Liu, B., Liu, K., Yan, J., Ostadhassan, M., 2022. An insight into core flooding experiment via NMR imaging and numerical simulation. Fuel 318, 123589. https://doi.org/10.1016/j.fuel.2022.123589.

Skauge, A., Solbakken, J., Ormehaug, P.A., Aarra, M.G., 2020. Foam generation, propagation and stability in porous medium. Transport Porous Media 131 (1), 5–21. https://doi.org/10.1007/s11242-019-01250-w.

Sun, L., Chen, W., 2022. Impact of carbon tax on CCUS source-sink matching: finding from the improved ChinaCCS DSS. J. Clean. Prod. 333, 130027. https://doi.org/10.1016/j.jclepro.2021.130027.

Talebian, S.H., Masoudi, R., Tan, I.M., Zitha, P.L.J., 2014. Foam assisted CO_2-EOR: a review of concept, challenges, and future prospects. J. Petrol. Sci. Eng. 120, 202–215. https://doi.org/10.1016/j.petrol.2014.05.013.

Tang, M., Wang, C., Yang, H., Lu, J., Yu, H., 2022. Experimental investigation on plugging performance of nanospheres in low-permeability reservoir with bottom water. Adv. Geo-Energy Res. 6 (2), 95–103. https://10.46690/ager.2022.02.02.

Tang, M., Zhang, T., Ma, Y., Hao, D., Yang, X., Li, Y., 2023. Experimental study on fracture effect on the multiphase flow in ultra-low permeability sandstone based on LF-NMR. Geoenergy Sci. Eng. 222, 211399. https://doi.org/10.1016/j.geoen.2022.211399.

Telmadarreie, A., Doda, A., Trivedi, J.J., Kuru, E., Choi, P., 2016. CO_2 microbubbles—a potential fluid for enhanced oil recovery: bulk and porous media studies.

J. Petrol. Sci. Eng. 138, 160–173. https://doi.org/10.1016/j.petrol.2015.10.035.
Telmadarreir, A., Doda, A., Trivedi, J.J., Kuru, E., Choi, P., 2016. CO_2 microbubbles – a potential fluid for enhanced oil recovery: bulk and porous media studies. J. Petrol. Sci. Eng. 138, 160–173. https://10.1016/j.petrol.2015.10.035.
Wang, S., Li, S., Liu, D., Shi, M., Tong, B., Cheng, C., Jiang, L., Song, Y., 2023. Study of the impact of various porous media on pore space utilization and CO_2 storage by injection of microbubbles into oil reservoirs. Appl. Energy 339, 120947. https://doi.org/10.1016/j.apenergy.2023.120947.
Wang, X., Geng, J., Zhang, D., Xiao, W., Chen, Y., Zhang, H., 2022. Influence of sub-supercritical CO_2 on pore structure and fractal characteristics of anthracite: an experimental study. Energy 261, 125115. https://doi.org/10.1016/j.energy.2022.125115.
Wei, B., Zhang, X., Wu, R., Zou, P., Gao, K., Xu, X., Pu, W., Wood, C., 2019. Pore-scale monitoring of CO_2 and N_2 flooding processes in a tight formation under reservoir conditions using nuclear magnetic resonance (NMR): a case study. Fuel 246, 34–41. https://doi.org/10.1016/j.fuel.2019.02.103.
Xiao, W., Ren, J., Pu, W., Yuan, C., Meng, L., Zheng, L., Zhao, H., Cheng, Q., 2023. Laboratory tests and field pilot of foam-assisted deoxidized-air flooding in a low-permeability sandstone reservoir. Fuel 352, 129150. https://doi.org/10.1016/j.fuel.2023.129150.
Xie, B., Zhou, C., Sang, L., Ma, X., Zhang, J., 2021. Preparation and characterization of microbubbles with a porous ceramic membrane. Chem. Eng. Process. Process Intensif. 159, 108213. https://doi.org/10.1016/j.cep.2020.108213.
Xue, Z., Nishio, S., Hagiwara, N., Matsuoka, T., 2014. Microbubble carbon dioxide injection for enhanced dissolution in geological sequestration and improved oil recovery. Energy Proc. 63, 7939–7946. https://doi.org/10.1016/j.egypro.2014.11.828.
Xue, Z., Yamada, T., Matsuoka, T., Kameyama, H., Nishio, S., 2011. Carbon dioxide microbubble injection–Enhanced dissolution in geological sequestration. Energy Proc. 4, 4307–4313. https://doi.org/10.1016/j.egypro.2011.02.381.
Yoon, R.-H., Yordan, J.L., 1986. Zeta-potential measurements on microbubbles generated using various surfactants. J. Colloid Interface Sci. 113 (2), 430–438. https://doi.org/10.1016/0021-9797(86)90178-5.
Yu, H., Fu, W., Zhang, Y., Lu, X., Cheng, S., Xie, Q., Qu, X., Yang, W., Lu, J., 2021a. Experimental study on EOR performance of CO_2-based flooding methods on tight oil. Fuel 290, 119988. https://doi.org/10.1016/j.fuel.2020.119988.
Yu, H., Rui, Z., Chen, Z., Lu, X., Yang, Z., Liu, J., Qu, X., Patil, S., Ling, K., Lu, J., 2019. Feasibility study of improved unconventional reservoir performance with carbonated water and surfactant. Energy 182, 135–147. https://doi.org/10.1016/j.energy.2019.06.024.
Yu, H., Xu, H., Fu, W., Lu, X., Chen, Z., Qi, S., Wang, Y., Yang, W., Lu, J., 2021b. Extraction of shale oil with supercritical CO_2: effects of number of fractures and injection pressure. Fuel 285, 118977. https://doi.org/10.1016/j.fuel.2020.118977.
Zhai, H., Xue, Z., Park, H., Aizawa, Y., Baba, Y., Zhang, Y., 2020. Migration characteristics of supercritical CO_2 microbubble flow in the Berea sandstone revealed by voxel-based X-ray computed tomography imaging analysis. J. Nat. Gas Sci. Eng. 77, 103233. https://doi.org/10.1016/j.jngse.2020.103233.
Zhang, T., Tang, M., Ma, Y., Zhu, G., Zhang, Q., Wu, J., Xie, Z., 2022. Experimental study on CO_2/Water flooding mechanism and oil recovery in ultralow-permeability sandstone with online LF-NMR. Energy 252, 123948. https://doi.org/10.1016/j.energy.2022.123948.
Zhang, Y., Gao, M., You, Q., Fan, H., Li, W., Liu, Y., Fang, J., Zhao, G., Jin, Z., Dai, C., 2019. Smart mobility control agent for enhanced oil recovery during CO_2 flooding in ultra-low permeability reservoirs. Fuel 241, 442–450. https://doi.org/10.1016/j.fuel.2018.12.069.